Electronic Self-Organization in the Single-Layer Manganite $Pr_{1-x}Ca_{1+x}MnO_4$

F. Ye,[1,*] Songxue Chi,[2] J. A. Fernandez-Baca,[1,2] A. Moreo,[2,3] E. Dagotto,[2,3] J. W. Lynn,[4] R. Mathieu,[5] Y. Kaneko,[5] Y. Tokura,[5,6,7] and Pengcheng Dai[2,1]

[1]*Neutron Scattering Science Division, Oak Ridge National Laboratory, Oak Ridge, Tennessee 37831-6393, USA*
[2]*Department of Physics and Astronomy, The University of Tennessee, Knoxville, Tennessee 37996-1200, USA*
[3]*Materials Science and Technology Division, Oak Ridge National Laboratory, Oak Ridge, Tennessee 37831-6393, USA*
[4]*NIST Center for Neutron Research, Gaithersburg, Maryland, 20899, USA*
[5]*ERATO Spin Superstructure Project and Multiferroics Project, JST, Tokyo 113-8656, Japan*
[6]*Cross-Correlated Materials Research Group (CMRG), RIKEN Advanced Science Institute, Wako 351-0198, Japan*
[7]*Department of Applied Physics, University of Tokyo, Tokyo 113-8656, Japan*

(Received 2 April 2009; published 14 October 2009)

We use neutron scattering to investigate the doping evolution of the magnetic correlations in the single-layer manganite $Pr_{1-x}Ca_{1+x}MnO_4$, away from the $x = 0.5$ composition where the CE-type commensurate antiferromagnetic (AF) structure is stable. We find that short-range incommensurate spin correlations develop as the system is electron doped ($x < 0.5$), which coexist with the CE-type AF order. This suggests that electron doping in this system induces an inhomogeneous electronic self-organization, where commensurate AF patches with $x = 0.5$ are separated by electron-rich domain walls with short-range magnetic correlations. This behavior is strikingly different than for the perovskite $Pr_{1-x}Ca_xMnO_3$, where the long-range CE-type commensurate AF structure is stable over a wide range of electron or hole doping around $x = 0.5$.

DOI: 10.1103/PhysRevLett.103.167202 PACS numbers: 75.47.Lx, 75.25.+z, 75.30.Kz

Understanding how electrons are distributed in narrow bandwidth manganese oxides remains one of the most intriguing unresolved problems in the physics of colossal magnetoresistance (CMR) manganites [1]. In the perovskite $R_{1-x}Ca_xMnO_3$ (R = rare earth ions) and single-layer $R_{1-x}Ca_{1+x}MnO_4$ manganites (the $n = \infty$ and $n = 1$ end members of the Ruddlesden-Popper series $R_{n(1-x)}Ca_{nx+1}Mn_nO_{3n+1}$ manganese oxides), the orbitals and magnetic spins of the Mn ions order at low temperature at the doping level $x = 0.5$, and form a checkerboardlike pattern, resulting in a commensurate (CM) antiferromagnetic (AF) CE structure [2–4]. Our research here clarifies what occurs in the manganites near $x = 0.5$ when their structures evolve from the three-dimensional (3D) perovskite to the single-layer structure which is the most two-dimensional (2D) member of the Ruddlesden-Popper series. Are novel charge-ordered states formed, or do the excess of electrons or holes become randomly distributed and localized, or does a self-organization occur involving mixed-phase tendencies? In the 3D perovskite manganites such as $Pr_{1-x}Ca_xMnO_3$ [5,6], the CE-type orbital and magnetic order persist in a wide doping range ($0.3 < x < 0.7$). Doping this system away from $x = 0.5$ to form $Pr_{0.7}Ca_{0.3}MnO_3$ induces a ferromagnetic component below the AF CE-ordering temperature [7]. This has been interpreted as evidence for phase coexistence involving ferromagnetic clusters and the AF CE structure [8], although the data are also consistent with a canted antiferromagnet [9,10].

In the case of the single-layer $La_{1-x}Sr_{1+x}MnO_4$ (LSMO), extensive neutron and x-ray scattering experiments [3,4,11–13] have shown that the system at $x = 0.5$ has a checkerboard charge ordering–orbital ordering (CO-OO) and a CE-type spin configuration similar to that of the perovskite manganites. However, as soon as electrons are doped into the $x = 0.5$ compound, the CE spin structure is destroyed and the system behaves like a spin glass while CO-OO is maintained [4]. But is this a generic feature or does it depend on the bandwidth and electron-phonon coupling of the material?

In this Letter, we report a systematic neutron scattering study of the magnetic correlations in the single-layer manganite $Pr_{1-x}Ca_{1+x}MnO_4$ (PCMO). Contrary to LSMO, electron doping into the $x = 0.5$ PCMO [14–16] is found to suppress, but not fully eliminate, the commensurate CE AF order. In addition, a set of new incommensurate (ICM) magnetic peaks are observed near the CM scattering from the CE structure. These results are compatible with a self-organized mixed-phase scenario where the state at $x < 0.5$ is composed of CE patches separated by electron-rich but magnetically disordered domain walls (Fig. 1). This result establishes potentially interesting analogies between the doping of some Cu oxide cuprates that leads to inhomogeneous electron distribution, and the doping of the CE state in manganites that also seems to induce electron-rich domain walls.

Single crystals of PCMO (mass $\approx$ 4 to 6 grams) were grown using the floating zone method. The phase purity and cation concentrations were checked by neutron, x-ray powder diffraction and inductively coupled plasma atomic emission spectroscopy, no noticeable composition defect was found. At room temperature, PCMO has an ortho-

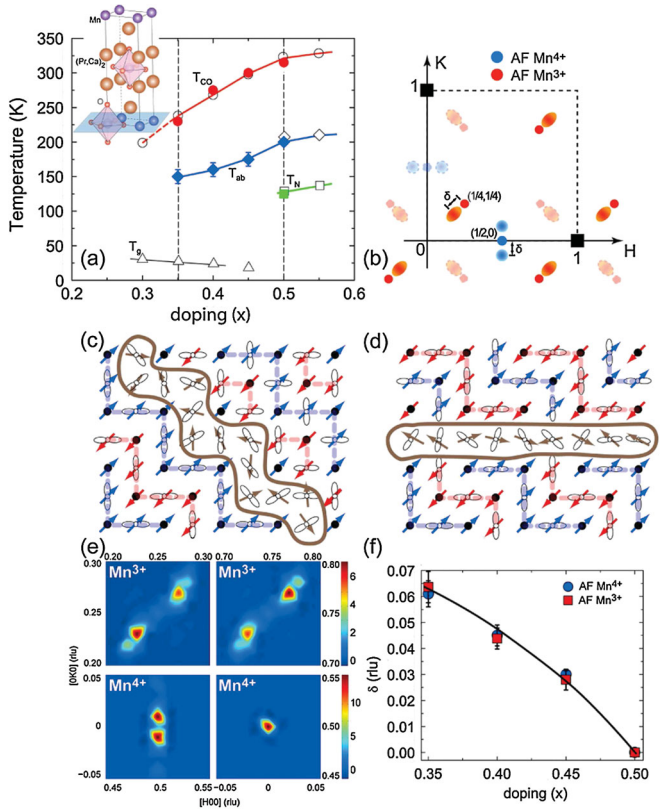

FIG. 1 (color). (a) Phase diagram of $Pr_{1-x}Ca_{1+x}MnO_4$. Solid symbols are from our measurements, open symbols from Ref. [15]. T_{CO} denotes the transition temperature of CO-OO, T_{ab} and T_N are the transition temperatures of 2D and 3D AF order. (b) Schematics of the experimental observations in reciprocal space. The pattern in lighter color originates from the 90° twinned domain. Orbital and spin configurations within the MnO_2 plane that may explain the neutron results: (c) are diagonal and (d) horizontal domain walls, where extra electrons congregate. Mn^{4+} ions are denoted by black circles. The Jahn-Teller active Mn^{3+} ions have additional orbitals. The blue and red lines illustrate the ferromagnetic zigzag spin chains which are coupled antiferromagnetically. (e) Fourier transform of the spin configurations in (c) and (d) combined. Note the dominant spectral weight at $(1/4 - \delta/\sqrt{2}, 1/4 - \delta/\sqrt{2})$ or $(3/4 + \delta/\sqrt{2}, 3/4 + \delta/\sqrt{2})$ for the Mn^{3+} spins. (f) Experimentally observed doping dependence of incommensurability from both the Mn^{3+} and Mn^{4+} sublattices.

rhombic structure slightly distorted from the tetragonal symmetry, with lattice parameters $a \approx 5.38$ Å, $b \approx 5.40$ Å, and $c \approx 11.85$ Å. For simplicity, we use the tetragonal unit cell ($a = b \approx 3.84$ Å). The experiments were carried out using triple-axis spectrometers at the NIST Center for Neutron Research with final neutron energy fixed at $E_f = 14.7$ or 13.5 meV. The momentum transfers $q = (q_x, q_y, q_z)$ in units of $Å^{-1}$ are at positions $(h, k, l) = (q_x a/2\pi, q_y b/2\pi, q_z c/2\pi)$ in reciprocal lattice units.

Figures 1(a) and 1(b) summarize the main results of our neutron scattering measurements. In $Pr_{0.5}Ca_{1.5}MnO_4$, the Mn spins form two magnetic sublattices. Compatible with a CE state, the characteristic wave vector associated with the Mn^{3+} spins appears at $q_1 = (1/4, /1, 4, 0)$ and the corresponding wave vector for the Mn^{4+} spins is at $q_2 = (1/2, 0, 0)$. However, the electron doping of $Pr_{0.5}Ca_{1.5}MnO_4$ induces additional ICM spin correlations at $(1/4 - \delta/\sqrt{2}, 1/4 - \delta/\sqrt{2}, 0)$ and $(1/2, \pm\delta, 0)$, respectively. The incommensurability (defined as the distance δ between the CM and the ICM peaks) of both sublattices shows a robust doping dependence [Fig. 1(f)].

Figure 2 shows the evolution of the magnetic scattering from the Mn^{3+} sublattice for the doped samples. A wide range of reciprocal space near the Bragg point (1/4, 1/4, 0) and equivalent positions in higher Brillouin zones was surveyed. At $x = 0.35$, the additional scattering consists of two parts. First, magnetic scattering is located at positions identical to those observed at $x = 0.50$ [14], but with weaker magnetic correlations between MnO_2 planes along the c axis. Second, there is ICM scattering at wave vector $(1/4 - \delta/\sqrt{2}, 1/4 - \delta/\sqrt{2}, 0)$. This scattering becomes strongest near (3/4, 1/4, 0) and decreases in intensity near (3/4, 3/4, 0). The ICM scattering is highly anisotropic with a rodlike profile elongated along the [1,1,0] (longitudinal) direction indicating a shorter correlation length in this direction. As the doping evolves toward $x = 0.5$, the diffusive ICM scattering sharpens and gradually moves towards the CM position. At $x = 0.45$, the scattering remains anisotropic, but the difference between the two orthogonal directions becomes smaller. As displayed in the wave vector scans, the longitudinal scan shows a broader width when compared to the transverse scan along the [1,1,0] direction. The corresponding correlation lengths ξ_L and ξ_T from the ICM scattering, after deconvoluting the

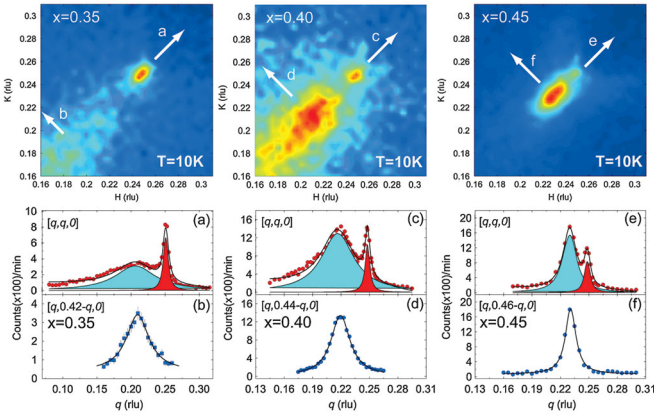

FIG. 2 (color). Comparison of the low-T magnetic scattering originating from the Mn^{3+} spins, for the $x = 0.35$, $x = 0.40$, and $x = 0.45$ samples. The corresponding wave vector scans through the peaks, as indicated by the arrows, are presented in the lower panels. The data reveal that a separate ICM component develops as electrons are added from the $x = 0.5$ point, which coexists with the $x = 0.5$ AF order. The ICM scattering is short range, and separates further from the CM position and becomes broader as x is reduced.

TABLE I. Doping dependence of the magnetic scattering correlation length ξ from the Mn^{3+} and Mn^{4+} sublattices. "L" and "T" denote the longitudinal and transverse directions.

$Pr_{1-x}Ca_{1+x}MnO_4$	$x = 0.35$	$x = 0.40$	$x = 0.45$
$\xi_L(Mn^{3+})$(Å)	12.2 ± 0.3	21.1 ± 0.4	52.5 ± 1.5
$\xi_T(Mn^{3+})$(Å)	20.2 ± 0.4	37.6 ± 0.9	66.5 ± 1.8
$\xi_{CM}(Mn^{3+})$(Å)	116.8 ± 4.5	139.4 ± 6.4	127.1 ± 6.6
$\xi_{ICM}(Mn^{4+})$(Å)	9.8 ± 1.1	15.9 ± 1.3	44.6 ± 1.4
$\xi_{CM}(Mn^{4+})$(Å)	131.4 ± 2.8	127.3 ± 5.3	121.0 ± 7.2

instrumental resolution, are listed in Table I. Both numbers increase substantially as the doping approaches $x = 0.5$.

The contour plots and the wave vector scans of the Mn^{4+} spins probed near $q_2 = (1/2, 0, 0)$ are illustrated in Fig. 3. The intense peaks at CM positions are surrounded by broad diffuse scattering. The CM component is sharper than the ICM fluctuations, but the Lorentzian profiles in the wave vector scans indicate the lack of true long-range order. Similar to the Mn^{3+} sublattice, the incommensurability of the diffuse scattering can be tuned by sample composition. As the ICM peaks move closer to the CM position with increasing x, the width of the diffuse peak narrows and the intensities become enhanced. The short-range correlations are less anisotropic than those in the Mn^{3+} sublattice.

To further characterize the magnetic correlations, we investigate the T dependence of the wave vector scans at $x = 0.45$ in Figs. 4(a) and 4(b). At $T = 10$ K, distinct CM and ICM peaks are observed. Upon warming, the amplitude of the ICM peak is rapidly suppressed with little variation in peak position and the scattering evolves into a broad feature as the temperature is raised. The scattering profile of the CM component, on the other hand, remains well resolved to a much higher temperature. The concave shape of the peak intensity vs temperature from the ICM scattering [Figs. 4(c) and 4(d)] reveals the expected diffusive nature for the short-range correlations, in contrast to the order-parameter-like CM scattering.

The suppression of the long-range CE magnetic order and the surprising emergence of the ICM spin fluctuations in PCMO are different from the insulating perovskite $Pr_{1-x}Ca_xMnO_3$, where the CE-type spin order survives over a broad carrier doping range [6]. Our results suggest a form of electronic self-organization in this single-layer compound. One might speculate that the ICM scattering results from the formation of an ICM charge density wave, with an associated spin density wave [17]. In this picture, the overall magnetic structure would resemble the usual CE-type checkerboard spin configuration, but the amplitudes of the spins would have a smooth spatial modulation to accommodate the extra electrons. While such a configuration naturally brings about the ICM magnetic peaks, they should be symmetric with respect to the CM positions [18] and the CE peaks should be absent, in contrast to the experimental observations. An alternative model consists of a mixed phase of the CE structure and the competing ferromagnetic state. There is ample evidence of this mixed

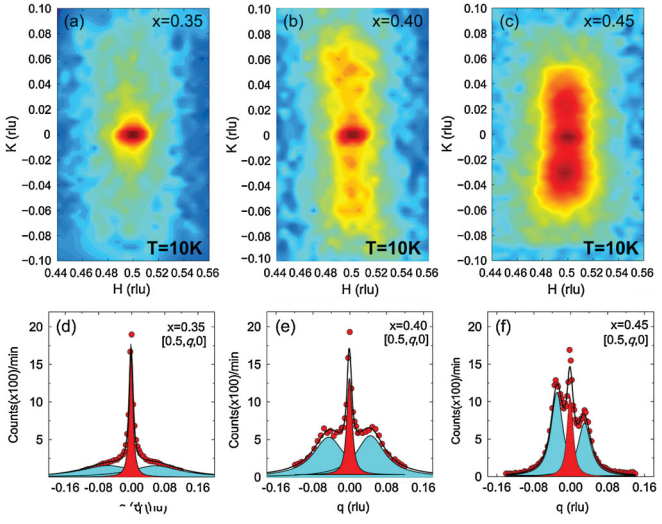

FIG. 3 (color). Comparison of the magnetic diffuse scattering originating from the Mn^{4+} spins at $T = 10$ K for the (a) $x = 0.35$, (b) $x = 0.40$, and (c) $x = 0.45$ samples. Wave vector scans across the ICM and CM peaks are in the panels (d)–(f).

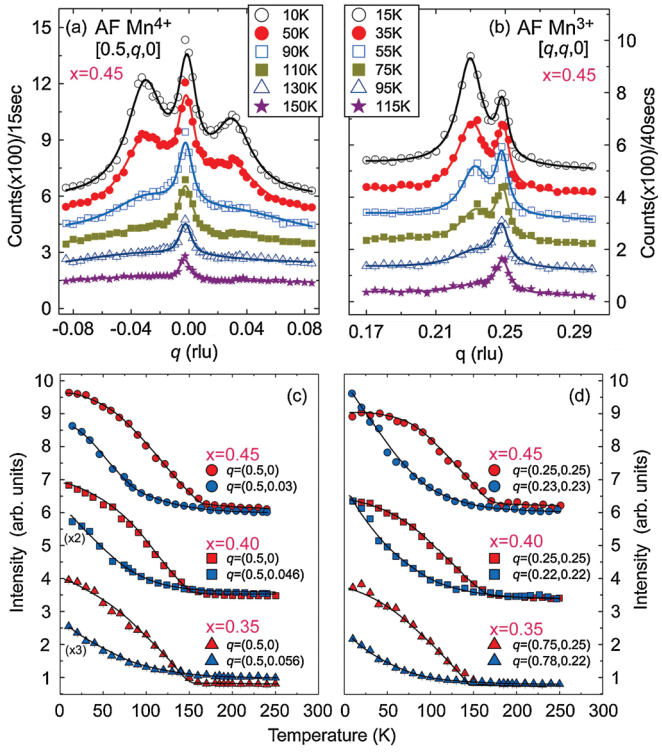

FIG. 4 (color). Wave vector scans of magnetic diffuse scattering from (a) Mn^{4+} and (b) Mn^{3+} sublattices of the $x = 0.45$ sample at selected temperatures. Temperature dependence of the CM (red) and ICM (blue) peak intensities from the (c) Mn^{4+} and (d) Mn^{3+} sublattices for $x = 0.35$, 0.40, and 0.45.

state in the CMR regime near the Curie temperature [9,10]. However, the present case is for low temperatures, and more importantly, we do not observe any ferromagnetic scattering. Therefore phase separation involving large size CE and FM clusters does not provide an explanation of our results either.

A model that is consistent with the overall experimental observations involves the formation of a stripe phase similar to those in the high-T_c superconducting cuprates [19]. For doping below $x = 0.5$, the system would form magnetic clusters or domains which preserve the CE-type spin configuration with distinct neighboring Mn^{3+} and Mn^{4+} sites. The excess electrons would congregate at the domain boundaries with random spin and orbital orientations. We explored a variety of real-space spin arrangements and found two different ones that, when combined, characterize the observations. The first one [Fig. 1(c)] describes a diagonal Mn^{3+} domain boundary separating two CE clusters in which the Mn^{3+} spins are in antiphase while the Mn^{4+} spins are not. The individual magnetic domain contributes to the CM scattering, while the ICM peak along the diagonal arises from the correlation between domains [20]. This configuration reproduces the magnetic scattering originating from the Mn^{3+} sites, but leaves the scattering near (1/2, 0, 0) undisturbed. The second one [Fig. 1(d)] describes spin arrangements with a horizontal domain boundary. There is an extra phase shift (1/4 or 3/4 of the $4a_c$, the periodicity of the CE phase) between adjacent magnetic domains. It introduces two symmetric ICM peaks at $q = (1/2, \pm\delta, 0)$ but not at $q = (0, 1/2 \pm \delta, 0)$. As demonstrated in Fig. 1(e), the Fourier transformation of the above described combined configurations successfully creates a pattern qualitatively similar to the experimental results [21]. Our identification of the inhomogeneous and textured spin states unveils another degree of similarity with the cuprates in terms of electronic self-organization and spin incommensurability [22], and provides a useful comparison to investigate the competing order and complexity in the strongly correlated electron system.

It was pointed out that the quenched disorder is important in determining the stability of the CE-type magnetic phase [23]. Monte Carlo simulations suggest that a small amount of disorder or randomness in 2D or 3D systems may destroy that phase. However, the inherent quenched disorder [24] in PCMO caused by A-site solid solution is small ($1 \sim 2 \times 10^{-7}$ for the doping range we studied) because of their comparable Pr^{3+}/Ca^{2+} ionic size. Therefore, the preservation of CE-type fluctuations at lower doping in PCMO confirms that the CE phase could be a robust feature, in contrast to its quick disappearance in LSMO with more quenched disorder [4]. On the other hand, the striking difference between single-layer PCMO and the 3D perovskite manganites highlights the crucial role of the magnetic interactions between planes, which is believed to stabilize the CE-type order [12,25].

We are grateful to D. Khomskii, Y. Ren, and M. Braden for their helpful discussions. The experimental work was partially supported by the Division of Scientific User Facilities of the Office of Basic Energy Sciences, U.S. Department of Energy and by the U.S. NSF DMR-0756568 and DOE No. DE-FG02-05ER46202 grants. The theory effort was supported by the NSF grant No. DMR-0706020, and by the Division of Materials Sciences and Engineering, U.S. DOE under contract with UT-Battelle, LLC.

*yef1@ornl.gov

[1] E. Dagotto *et al.*, Phys. Rep. **344**, 1 (2001); M. Salamon and M. Jaime, Rev. Mod. Phys. **73**, 583 (2001).
[2] E. O. Wollan and W. C. Koehler, Phys. Rev. **100**, 545 (1955); John B. Goodenough, Phys. Rev. **100**, 564 (1955).
[3] B. J. Sternlieb *et al.*, Phys. Rev. Lett. **76**, 2169 (1996).
[4] S. Larochelle *et al.*, Phys. Rev. Lett. **87**, 095502 (2001).
[5] Z. Jirák *et al.*, J. Magn. Magn. Mater. **53**, 153 (1985).
[6] Y. Tomioka *et al.*, Phys. Rev. B **53**, R1689 (1996).
[7] H. Yoshizawa *et al.*, J. Phys. Soc. Jpn. **65**, 1043 (1996); R. Kajimoto *et al.*, Phys. Rev. B **58**, R11837 (1998).
[8] A. Moreo *et al.*, Science **283**, 2034 (1999); J. Burgy *et al.*, Phys. Rev. Lett. **92**, 097202 (2004); H. Sha *et al.*, Phys. Rev. B **78**, 052410 (2008).
[9] H. Yoshizawa *et al.*, Phys. Rev. B **52**, R13145 (1995).
[10] J. A. Fernandez-Baca *et al.*, Phys. Rev. B **66**, 054434 (2002).
[11] S. Larochelle *et al.*, Phys. Rev. B **71**, 024435 (2005).
[12] D. Senff *et al.*, Phys. Rev. Lett. **96**, 257201 (2006).
[13] D. Senff *et al.*, Phys. Rev. B **77**, 184413 (2008).
[14] Songxue Chi *et al.*, Proc. Natl. Acad. Sci. U.S.A. **104**, 10796 (2007).
[15] R. Mathieu and Y. Tokura, J. Phys. Soc. Jpn. **76**, 124706 (2007).
[16] X. Z. Yu *et al.*, Phys. Rev. B **75**, 174441 (2007).
[17] J. C. Loudon *et al.*, Phys. Rev. Lett. **94**, 097202 (2005).
[18] A homogeneous incommensurate spin configuration for the Mn^{4+} ions in the CE pattern that produces peaks in the structure factor at $(1/2, \pm\delta, 0)$ as in Fig. 3 arises from correlation functions that in real space have the form $S(x, y, 0) = A(-1)^x \cos(\delta y)$. However, a Fourier transform of this expression produces a structure factor with peaks at $(1/2, \pm\delta, 0)$ and also at $(0, 1/2 \pm \delta, 0)$ which is not observed in the experiments.
[19] J. M. Tranquada *et al.*, Nature (London) **375**, 561 (1995).
[20] A small amount of disorder to the spin orientations about the CE state has been added to make the system more realistic but similar results are obtained without disorder.
[21] Note that our model combines two configurations "incoherently." A more complicate "coherent" model might reveal other novel features (like extra satellite peaks) and deserves future investigation.
[22] N. Mannella *et al.*, Nature (London) **438**, 474 (2005).
[23] G. Alvarez *et al.*, Phys. Rev. B **73**, 224426 (2006).
[24] This is characterized by $\sigma^2 = \sum_i (x_i r_i^2 - \bar{r}^2)$, where x_i is the fractional occupancies of A-site species, r_i and $\bar{r} = \sum_i x_i r_i$ are individual radii and averaged ionic radius.
[25] C. Ma *et al.*, J. Phys. Condens. Matter **21**, 045601 (2009).